135GHz CMOS / LTCC MIMO Receiver Array Tile Modules

Ali A. Farid¹, A. S. H. Ahmed¹, A Dhananjay², Panagiotis Skrimponis², Sundeep Rangan², Mark Rodwell¹

¹Department of Electrical and Computer Engineering University of California, Santa Barbara, USA

²Pi-Radio Inc., 155 Water Street Unit 4/10, Brooklyn, 11201 NY, USA

³Tandon School of Engineering, New York University

afarid@ece.ucsb.edu

Abstract—We report 135GHz MIMO receiver array tile modules. The module integrate four or eight RF channels on an LTCC carrier, each channel having a 22nm SOI CMOS IC for RF-baseband and a linear microstrip patch antenna array; DC, baseband IQ and LO reference signal connections are by printed circuit board connected to the LTCC carrier. Digital beamforming is demonstrated with the 8-element array, showing 12° 3-dB beam width and 56° angular steering range, and with the 4-element array, showing 12° 3-dB beam width and 20° angular steering range before the appearance of grating lobes. The 4-element arrays, in single-beam operation, shows -15.7 dB RMS error vector magnitude receiving 1.34Gb/s QPSK data, and shows -15.6dB error vector magnitude receiving 1.92Gb/s 16QAM data.

Keywords—Heterogeneously integrated receivers, D-band receiver, MIMO receiver, millimeter wave packaging. .

I. INTRODUCTION

100-300GHz wireless systems will benefit from large available bandwidths and, given the short wavelengths, which permit compact transceiver arrays with many elements, massive spectral re-use via massive spatial multiplexing (MIMO). Extremely high link capacities are feasible [1] in endpoint and backhaul links; endpoint links provide data transmission between a hub and many mobile or fixed users, while backhaul links transmit data from the hubs to the internet backbone.

Reported D-band (110-170GHz) receivers and transceivers include single-channel ICs [2,3,4,5,6], packaged single-channel transceivers [7, 8, 9], dual-polarization transceivers [10], a 143GHz outdoor link [11], a 2×2 line-of-sight MIMO link [12], a link using 4- and 16-element arrays [13], and array transceiver ICs [14]. Here we report receiver

hub array tile modules for a 135GHz MIMO endpoint link.

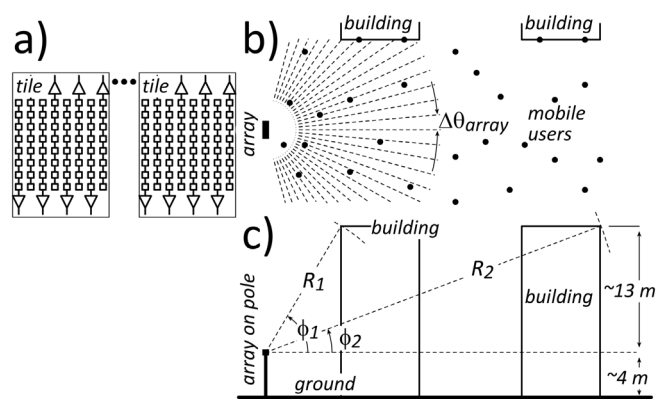


Figure 1: The array (a) tiles horizontally, producing horizontally-steered beams having narrow lateral and moderate vertical beam width. Users are primarily distributed laterally over the ground (b) but some distributed vertically in tall buildings (c). Given a maximum building height, the range R decreases rapidly as the elevation angle ϕ increases, hence vertical beam steering is not required.

II. APPLICATION, ARCHITECTURE, AND CONSTRUCTION

The receiver tile module is design for use in sets to form 32-element or larger horizontal linear array (Figure 1a) that simultaneously receives many incident signals, separating them (Figure 1b) by their horizontal angle of incidence θ . If most users are on the ground, with fewer in tall buildings, a linear (1D) array better separates user signals than a 2D array. Even with a small vertical -3dB beam width and no vertical beam steering, signals from the top of moderately tall buildings can be received because, given some maximum

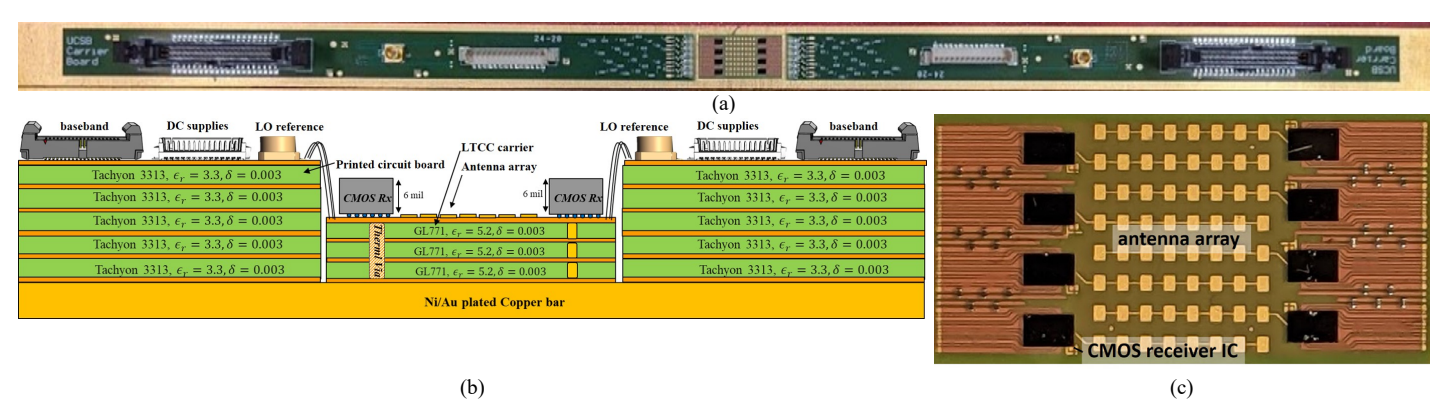


Figure 2: Eight-channel 140GHz MIMO receiver array tile module: (a) photograph of the overall module, (b) cross-section diagram showing the interface printed circuit boards, the LTCC carrier, connectors, and ICs, and (c) photograph of the LTCC carrier showing the antennas and CMOS ICs. The overall module is 450mm × 15mm, while the LTCC carrier is approximately 12 mm × 25 mm.

height, as the elevation angle ϕ increases, the received signal strength will *increase* if the antenna is designed so that its gain decreases less rapidly than $\sin^{-2}(\phi)$ at large ϕ .

The array is designed for use with MIMO digital beamforming [15,16,17], which, from the array's IQ output signals, determines the data and direction of the received signals. System link budget analysis is reported in [1].

Figure 2 shows photographs of the full module and of the assembled LTCC carrier, and shows a module cross-section. The module has an array of eight antennas, at 0.65λ pitch, each being a linear microstrip patch array. These antennas feed eight single-channel receiver ICs [3], in Global Foundries 22nm SOI CMOS that down convert the received RF signals, generating differential baseband IQ signals. Figure 3 shows a detailed block diagram.

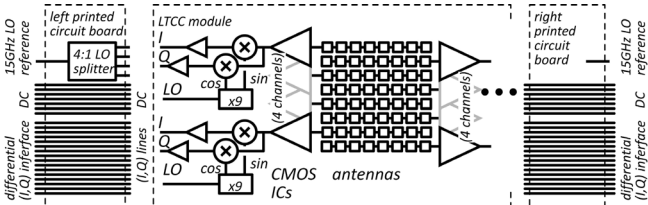


Figure 3: The MIMO receiver array tile module contains an LTCC carrier with eight receiver channels, each channel having a linear microstrip patch antenna array and a CMOS receiver IC, plus two printed circuit boards providing baseband IQ signal and DC connections, plus a 4:1 spitting network for the 15GHz LO reference signal.

The CMOS ICs are attached by flip-chip bonding using 50 µm Cu studs; [18] reports the design and performance of the antennas and flip-chip interfaces. The measured gain of a single element of the 8-element antenna array, itself an 8-element series-fed patch antenna, is 11dB, with 12° E-plane (vertical) and 70° H-plane (horizontal) 3-dB beam width. The horizontal beam width is then decreased by the array gain.

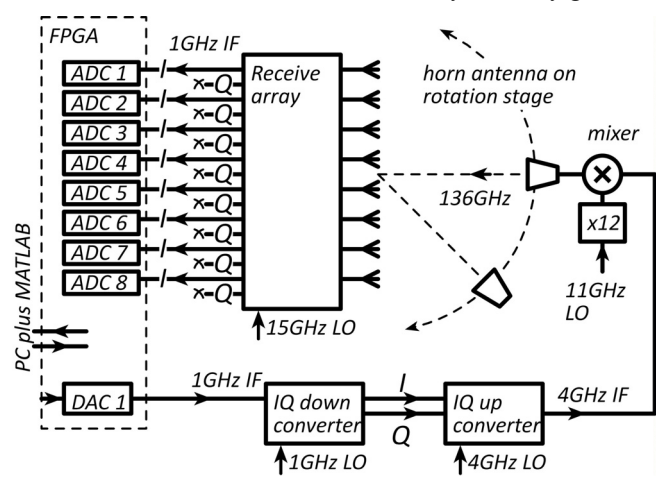


Figure 4: Experimental configuration for receiver array characterization. The FPGA generates modulated data on a 1GHz IF, an IQ downconverter and IQ upconverter then convert this to a 4GHz IF, and a mm-wave mixer translates this to 136GHz, with an 128GHz image outside the receiver passband. The test transmitter is mounted on a rotation stage 15cm from the array. The receiver array generates 1GHz IF signals, at quadrature phase between I and Q; the I-signals are captured by the FPGA.

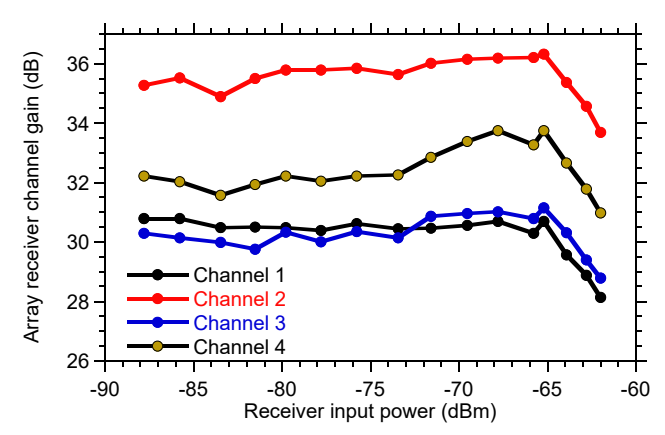


Figure 5: Measured gains of the receiver channels on the 4-channel module.

III. ARRAY CHARACTERIZATION

To test the arrays (Figure 4), a PC running MATLAB generates a numerical description of a 1GHz bandwidth OFDM waveform and transfers it to an FPGA, which generates the analog waveform on a 1GHz IF. An IQ downconverter (ADI ADL5380) and upconverter (ADI ADL5375) then shift the signal to a 4GHz IF. The signal is them mixed against a 132GHz LO to generate a 136GHz drive signal, plus an 128GHz image response that lies outside the receiver passband. A horn antenna, on a rotation stage at 15cm range, illuminates the array with the 136GHz drive signal. If the receiver were to convert its signals to baseband, then its 16 IQ outputs would have to be digitized, yet the FPGA only has eight ADCs. Instead, the receiver array LO is offset so that its outputs are at a 1GHz IF. The quadrature phase outputs are then redundant, and the eight array channels are monitored by the eight FPGA ADCs.

Two eight-channel receiver modules were constructed; both have assembly defects. In one, four of the eight channels function, resulting in a 4-element array at 1.3λ pitch. In the second, all eight channels function, but excessive DC supply lead resistance prevents proper biasing for high-data-rate operation. Figure 5 shows the gain, versus received power, for the channels on the 4-channel module.

To form and aim beams, the array must be calibrated, i.e. differences between channel gains and phases are measured and then corrected for. Given the significant differences between channel gains, only phase errors were calibrated. Device drivers and calibration procedures were adapted from Pi-Radio open-source code [19]. These first measure the perchannel fractional timing offsets of the received data streams and the channel-channel variations in the signal phase. The resulting calibration factors are applied to the receiver output signals to perform beamforming and data transmission. experiments.

Having calibrated the arrays, radiation patterns were then generated for the 4-element and 8-element arrays (Figure 6). In each measurement, the illuminating horn antenna is positioned at some particular angular of incidence, and the array then computes the received power as a function of direction. This demonstrates digital beamforming. The 4-

element array (Figure 6a) shows 12° 3-dB H-plane (horizontal) beam width, but, because of the 1.3λ element spacing, only 20° angular steering range before the appearance of grating lobes. The 8-element array shows 12° 3-dB H-plane (horizontal) beam width and over 56° angular steering range.

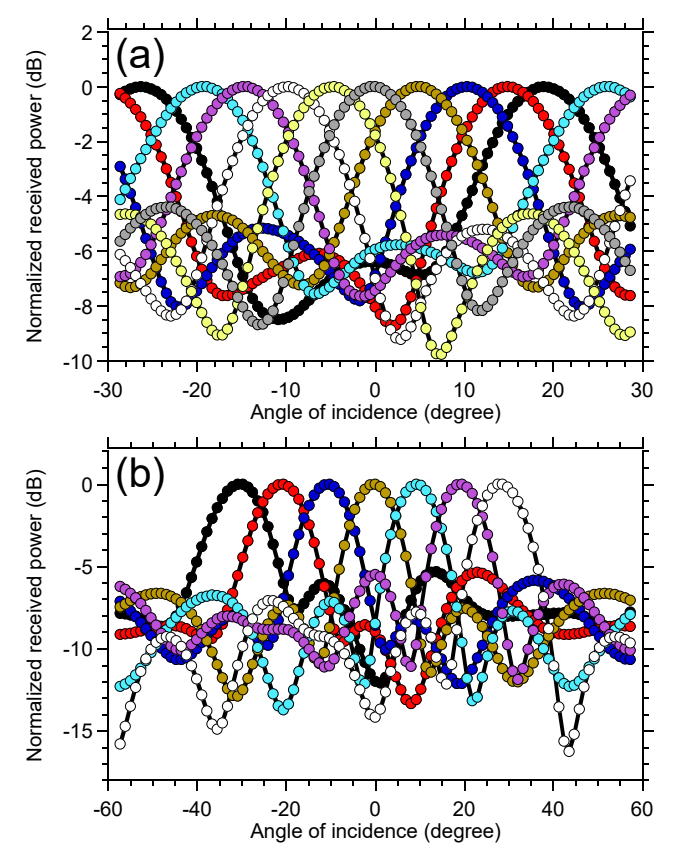


Figure 6: Measured array patterns for (a) the four-channel receiver, taken with the test transmitter located at nine different angular positions and (b) the eight-channel receiver, taken with the test transmitter located at seven different angular positions.

Figure 7 shows data transmission experiments. The data is transmitted using OFDM, with 960kHz subcarrier spacing. The constellation diagrams show the demodulated signal after frequency-domain OFDM equalization was performed. The pilot density is approximately 20%. In single-beam operation, there is -15.7dB RMS error vector magnitude in 1.34Gb/s QPSK transmission, and -15.6dB error vector magnitude in 1.92Gb/s 16QAM transmission. Figure 8 shows the error vector magnitude as a function of data rate.

Table 1 compares state-of-the-art packaged D-band (110-170GHz) multi-channel receivers and transmitter/receiver link demonstrations.

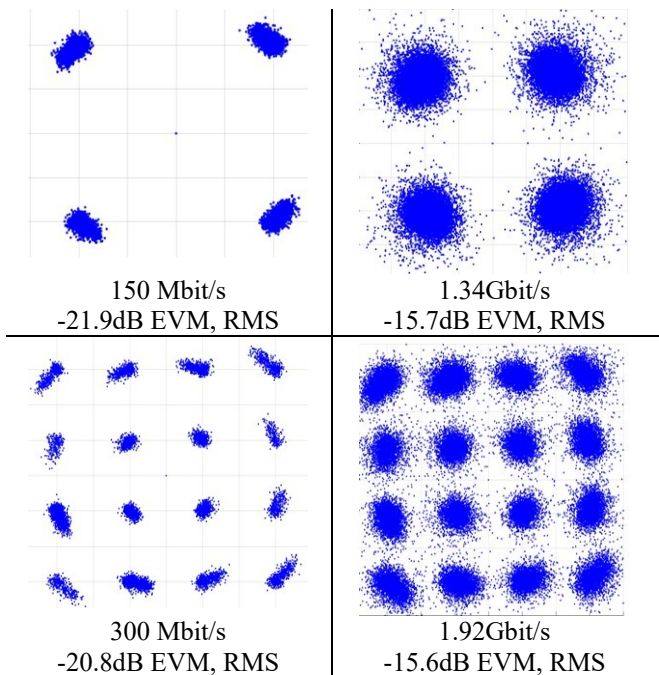


Figure 7: Measured receiver QPSK and 16QAM modulation constellations and computed error vector magnitude.

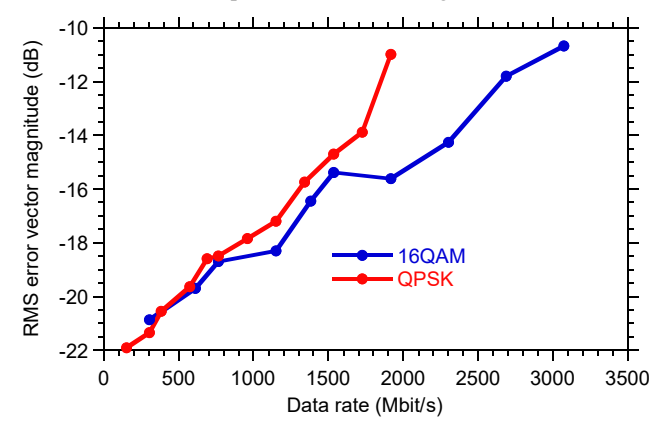


Figure 8: Computed error vector magnitude, in dB relative to the constellation's RMS amplitude, as a function of data rate.

Table 1. Comparison between state-of-the-art multi-channel receiver modules at D-frequency band (110-170GHz)

Result	[10]	[12]	[13]	[14]*	this work
Freq, GHz	113	135	140	130-170	140
IC	CMOS	SiGe	CMOS	SiGe	CMOS
Package	PCB	PCB and lenses	PCB	Glass	LTCC
Type	1-beam	2×2 LOS MIMO	MIMO ^{\$}	single-beam array	MIMO
TX/RX	TX,RX	TX, RX	TX, RX	TX, RX	RX
channels	2	2	4, 8,16	8*	4 (8)
Data	1× 80Gb/s	2× 16Gb/s	6Gb/s		1.34Gb/s 1.92Gbs
Format	16QAM	QPSK	16QAM		QPSK 16QAM
EVM					-15.7dB -15.6dB
Link	air	air	air		air
Distance	10cm	6cm	15m		15cm

[§]MIMO-compatible digital beamforming: 1 beam demonstrated

^{*}No experimental data shown for the array.

IV. CONCLUSIONS

We report a 8-channel MIMO hub receiver array tile module using CMOS receivers and a microstrip patch antenna array on an LTCC substrate. The module is designed to tile into larger arrays to serve high-data-rate endpoint links to multiple mobile users. Digital beamforming has been is demonstrated with the arrays, showing 12° 3-dB beam width and 56° angular steering range, and data transmission has been demonstrated at up to 1.92Gb/s. With the construction of several of these modules, high-capacity D-band MIMO hub receivers should be feasible.

ACKNOWLEDGMENT

This work was supported in part by the Semiconductor Research Corporation and DARPA under the JUMP program. The authors are grateful for Kyocera for fabrication of the ceramic carrier and for Kyocera San Diego for their assembly efforts. The authors would like to thank GlobalFoundries for the 22nm FDSOI chip fabrication and for the free access to GF advanced copper pillars. Thanks to Prof. Ali Niknejad and Anita Flynn of UC Berkeley for extensive guidance on the PCB and interface design, and to Gary Xu and Navneet Sharma of Samsung Research America for guidance and encouragement.

REFERENCES

- [1] M. J. W. Rodwell, "100-340GHz Spatially Multiplexed Communications: IC, Transceiver, and Link Design," 2019 IEEE 20th International Workshop on Signal Processing Advances in Wireless Communications (SPAWC), 2019, pp. 1-5, doi: 10.1109/SPAWC.2019.8815433.
- [2] A. Simsek, S. Kim and M. J. W. Rodwell, "A 140 GHz MIMO Transceiver in 45 nm SOI CMOS," 2018 IEEE BiCMOS and Compound Semiconductor Integrated Circuits and Technology Symposium (BCICTS), 2018, pp. 231-234, doi: 10.1109/BCICTS.2018.8550954.
- [3] A. A. Farid, A. Simsek, A. S. H. Ahmed and M. J. W. Rodwell, "A Broadband Direct Conversion Transmitter/Receiver at D-band Using CMOS 22nm FDSOI," 2019 IEEE Radio Frequency Integrated Circuits Symposium (RFIC), 2019, pp. 135-138, doi: 10.1109/RFIC.2019.8701730.
- [4] C. Wang, G Rebeiz "A 2-Channel 136-156 GHz Dual Down-Conversion I/Q Receiver with 30 dB Gain and 9.5 dB NF Using CMOS 22nm FDSOI", 2021 IEEE Radio Frequency Integrated Circuits Symposium (RFIC), Atlanta, GA, USA, 2021.
- [5] X. Tang, J. Nguyen, G. Mangraviti, Z. Zong, P. Wambacq"A 140 GHz T/R Front-End Module in 22 nm FD-SOI CMOS", 2021 IEEE Radio Frequency Integrated Circuits Symposium (RFIC), Atlanta, GA, USA.
- [6] S. Carpenter et al., "A \$D\$-Band 48-Gbit/s 64-QAM/QPSK Direct-Conversion I/Q Transceiver Chipset," in IEEE Transactions on

- Microwave Theory and Techniques, vol. 64, no. 4, pp. 1285-1296, April 2016, doi: 10.1109/TMTT.2016.2533491.
- [7] V. Vassilev et al., "Spectrum Efficient D-band Communication Link for Real-time Multi-gigabit Wireless Transmission," 2018 IEEE/MTT-S International Microwave Symposium - IMS, 2018, pp. 1523-1526, doi: 10.1109/MWSYM.2018.8439258.
- [8] M. Hörberg, Y. Li, V. Vassilev, H. Zirath and J. Hansryd, "A 143 GHz InP-Based Radio Link Characterized in Long-Term Outdoor Measurement," 2018 Asia-Pacific Microwave Conference (APMC), 2018, pp. 234-236, doi: 10.23919/APMC.2018.8617371.
- [9] I. Kallfass et al., "All Active MMIC-Based Wireless Communication at 220 GHz," in IEEE Transactions on Terahertz Science and Technology, vol. 1, no. 2, pp. 477-487, Nov. 2011, doi: 10.1109/TTHZ.2011.2160021.
- [10] A. Townley et al., "A Fully Integrated, Dual Channel, Flip Chip Packaged 113 GHz Transceiver in 28nm CMOS supporting an 80 Gb/s Wireless Link," 2020 IEEE Custom Integrated Circuits Conference (CICC), 2020, pp. 1-4, doi: 10.1109/CICC48029.2020.9075890.
- [11] M. Hörberg, Y. Li, V. Vassilev, H. Zirath and J. Hansryd, "A 143 GHz InP-Based Radio Link Characterized in Long-Term Outdoor Measurement," 2018 Asia-Pacific Microwave Conference (APMC), 2018, pp. 234-236, doi: 10.23919/APMC.2018.8617371.
- [12] M. Sawaby et al., "A Fully Integrated 32 Gbps 2x2 LoS MIMO Wireless Link with UWB Analog Processing for Point-to-Point Backhaul Applications," 2020 IEEE Radio Frequency Integrated Circuits Symposium (RFIC), 2020, pp. 107-110, doi: 10.1109/RFIC49505.2020.9218371.
- [13] S. Abu-Surra, W. Choi, S. Choi, E. Seok, D. Kim, N. Sharma, S. Advani, V. Loseu, K. Bae, I. Na, A. Farid, M. J. W. Rodwell, G. Xu, J. Zhang, "End-to-end 140 GHz Wireless Link Demonstration with Fully-Digital Beamformed System", IEEE International Conference on Communications, 14-23 June 2021, Montreal (virtual)
- [14] M. Elkhouly et al., "D-band Phased-Array TX and RX Front Ends Utilizing Radio-on-Glass Technology," 2020 IEEE Radio Frequency Integrated Circuits Symposium (RFIC), 2020, pp. 91-94, doi: 10.1109/RFIC49505.2020.9218409.
- [15] A. A. Farid, M. Abdelghany, U. Madhow and M. J. W. Rodwell, "Dynamic Range Requirements of Digital vs. RF and Tiled Beamforming in mm-Wave Massive MIMO," 2021 IEEE Radio and Wireless Symposium (RWS), 2021, pp. 46-48, doi: 10.1109/RWS50353.2021.9360362.
- [16] M. Abdelghany, U. Madhow and A. Tölli, "Beamspace Local LMMSE: An Efficient Digital Backend for mmWave Massive MIMO," 2019 IEEE 20th International Workshop on Signal Processing Advances in Wireless Communications (SPAWC), 2019, pp. 1-5, doi: 10.1109/SPAWC.2019.8815585.
- [17] S. H. Mirfarshbafan, A. Gallyas-Sanhueza, R. Ghods and C. Studer, "Beamspace Channel Estimation for Massive MIMO mmWave Systems: Algorithm and VLSI Design," in IEEE Transactions on Circuits and Systems I: Regular Papers, vol. 67, no. 12, pp. 5482-5495, Dec. 2020, doi: 10.1109/TCSI.2020.3023023.
- [18] A. Farid, A. S. H. Ahmed, A. Simsek, M. J. W. Rodwell, "A Packaged 135GHz 22nm FD-SOI Transmitter on an LTCC Carrier" IEEE International Microwave Symposium (IMS). 6-11 June, Atlanta and virtual
- [19] https://github.com/pi-radio/Pi-Radio-v1-NRT https://dl.acm.org/doi/abs/10.1145/3411276.3412195